QUANTUM PHYSICS

Quantum optical rotatory dispersion

Nora Tischler,[1,2,3]*† Mario Krenn,[1,2] Robert Fickler,[1,2]‡ Xavier Vidal,[3] Anton Zeilinger,[1,2] Gabriel Molina-Terriza[3]

The phenomenon of molecular optical activity manifests itself as the rotation of the plane of linear polarization when light passes through chiral media. Measurements of optical activity and its wavelength dependence, that is, optical rotatory dispersion, can reveal information about intricate properties of molecules, such as the three-dimensional arrangement of atoms comprising a molecule. Given a limited probe power, quantum metrology offers the possibility of outperforming classical measurements. This has particular appeal when samples may be damaged by high power, which is a potential concern for chiroptical studies. We present the first experiment in which multiwavelength polarization-entangled photon pairs are used to measure the optical activity and optical rotatory dispersion exhibited by a solution of chiral molecules. Our work paves the way for quantum-enhanced measurements of chirality, with potential applications in chemistry, biology, materials science, and the pharmaceutical industry. The scheme that we use for probing wavelength dependence not only allows one to surpass the information extracted per photon in a classical measurement but also can be used for more general differential measurements.

INTRODUCTION

The concept of chirality, which means that an object cannot be superposed onto its mirror image, pervades several fields of science, including chemistry, biology, physics, and materials science, and also plays a key role in the pharmaceutical industry (*1*, *2*). One of the means by which we can probe the chirality of molecules is through its effect on light-matter interaction, manifesting as the phenomena of optical activity and circular dichroism (*3*–*5*). Optical activity can be understood as circular birefringence, which results in a different phase for the two circular polarizations. Polarization-based phase estimation is amenable to techniques from quantum metrology that hold the possibility of beating the standard quantum limit and has been demonstrated in a number of quantum metrology experiments in the past (*6*–*15*). In one of these, Wolfgramm *et al.* (*12*) reported the measurement of Faraday rotation using a narrowband polarization NOON state. This suggests that nonclassical resources could also be exploited in chiroptical techniques, given that Faraday rotation and molecular optical activity have a similar effect on light despite their different physical origins. However, a new approach is needed to accommodate the significance of wavelength dependence in chiroptical techniques. Addressing this challenge, we show how entangled photons can be used to study optical activity as a function of wavelength, with an enhancement in the information about multiwavelength quantities that is extracted per photon. In particular, we will focus on the optical rotations for two wavelengths at a time, as illustrated in Fig. 1, and consider the mean and difference of the rotations, denoted by $\bar{\alpha}$ and $\Delta\alpha$, respectively.

[1]Vienna Center for Quantum Science and Technology, Faculty of Physics, University of Vienna, Boltzmanngasse 5, A-1090 Vienna, Austria. [2]Institute for Quantum Optics and Quantum Information, Austrian Academy of Sciences, Boltzmanngasse 3, A-1090 Vienna, Austria. [3]Department of Physics and Astronomy, Centre for Engineered Quantum Systems, Macquarie University, Sydney, New South Wales 2109, Australia.
*Present address: Centre for Quantum Dynamics, Griffith University, Brisbane 4111, Australia.
†Corresponding author. Email: nora.tischler@univie.ac.at
‡Present address: Department of Physics and Max Planck Centre for Extreme and Quantum Photonics, University of Ottawa, Ottawa, Ontario K1N 6N5, Canada.

RESULTS

Measurement scheme

The straightforward classical approach to measuring optical rotations at two wavelengths would be to simply perform a measurement at each wavelength. Given the resource of two photons, this could be implemented with a separable photon pair where each photon has linear polarization and measurements are performed in the horizontal-vertical (H-V) basis. We will use this as the classical benchmark to which the quantum metrology scheme may be compared. For the quantum scheme of our experiment, two different types of biphoton input states are used. In both cases, the two photons are in separate paths and may additionally have unequal wavelengths. The input states are the following polarization-entangled states

$$|\Phi_{\text{in}}\rangle \equiv \frac{1}{\sqrt{2}}\left[|R,\lambda_1\rangle_1|R,\lambda_2\rangle_2 + e^{i\alpha_0}|L,\lambda_1\rangle_1|L,\lambda_2\rangle_2\right] \quad (1)$$

$$|\Psi_{\text{in}}\rangle \equiv \frac{1}{\sqrt{2}}\left[|R,\lambda_1\rangle_1|L,\lambda_2\rangle_2 + e^{i\alpha_0}|L,\lambda_1\rangle_1|R,\lambda_2\rangle_2\right] \quad (2)$$

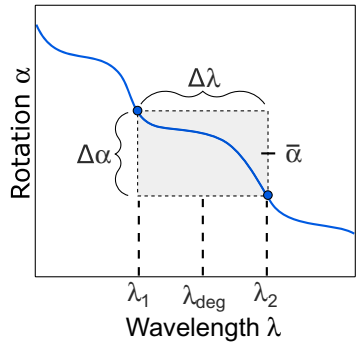

Fig. 1. Illustration of the two quantities that were measured with two types of input states. The state $|\Phi_{\text{in}}\rangle$ with correlated polarizations is sensitive to $\bar{\alpha}$, the mean of the optical rotations of the two wavelengths in question. In contrast, the state $|\Psi_{\text{in}}\rangle$ with anticorrelated polarizations is sensitive to $\Delta\alpha$, the difference of the two optical rotations. The curve is a fictitious example for illustration purposes.

Here, $|P, \lambda_1\rangle_1|P', \lambda_2\rangle_2$ is shorthand for the two-photon composite system. $|P, \lambda_m\rangle_m$ symbolizes a photon with polarization P and wavelength λ_m in path m. The polarization is L or R for left or right circular polarization, which implies a helicity of 1 and −1, respectively. The phase α_0 will be referred to as the bias phase, and the Bell states are recovered when $\alpha_0 = n\pi$, $n \in \mathbb{Z}$. Optical activity that is experienced by light passing through a solution of chiral molecules can be modeled as a unitary transformation of the form $U(\alpha(C, \lambda)) = \exp[-i\Lambda\alpha(C, \lambda)]$, where Λ is the helicity of the light and $\alpha(C, \lambda)$ is the angle by which the linear polarization of single photons is rotated, which is a function of the wavelength of the light λ and of the concentration of the solution C. The measurement parameters are $\bar{\alpha} \equiv \frac{1}{2}(\alpha(C, \lambda_1) + \alpha(C, \lambda_2))$ and $\Delta\alpha \equiv (\alpha(C, \lambda_2) - \alpha(C, \lambda_1))$. Using the quantum input states and projective measurements in the H-V basis, the expectation values of the HH and VV coincidences are $\frac{1}{4}(1 + \cos(\theta))$, whereas the mixed coincidences HV and VH yield $\frac{1}{4}(1 - \cos(\theta))$, where $\theta = \alpha_0 - 4(\bar{\alpha}(C, \lambda_1, \lambda_2))$ when $|\Phi_{in}\rangle$ is used and $\theta = \alpha_0 + 2(\Delta\alpha(C, \lambda_1, \lambda_2))$ for $|\Psi_{in}\rangle$.

To assess the performance of the measurement schemes, we make use of the Fisher information (FI), which is a measure of the information about a parameter that can be extracted from the probe state with a given measurement procedure. It is defined as

$$I(\theta) \equiv \sum_i p(x_i|\theta)\left(\frac{\partial \ln p(x_i|\theta)}{\partial\theta}\right)^2$$

where $p(x_i|\theta)$ is the probability of obtaining the measurement outcome x_i given the parameter value of θ, and the sum is taken over all measurement outcomes (which are HH, HV, VH, and VV in our experiment) of the positive operator–valued measure (POVM) (*16*). As detailed in section A of the Supplementary Materials, the two quantum input states distinguish themselves from the classical state through the interesting property that each is sensitive to one of the multiwavelength quantities, $\bar{\alpha}$ or $\Delta\alpha$, but is insensitive to the other. Using the state $|\Phi_{in}\rangle$ provides a factor of 2 enhancement of the FI for the estimation of the mean rotation $\bar{\alpha}$ compared to the classical scheme, whereas $|\Psi_{in}\rangle$ yields a factor of 2 enhancement for the estimation of the rotation difference $\Delta\alpha$. Furthermore, the FI is equal to the quantum Fisher information, which is the FI optimized over all possible POVMs (*17*, *18*). This shows that our projective measurement in the H-V basis is optimal.

Experimental implementation

The experimental setup with which we implemented the idea is shown in Fig. 2. A polarization-based Sagnac interferometer with type II spontaneous parametric down-conversion (SPDC) is used to create a polarization-entangled biphoton state (*19*, *20*), from which $|\Phi_{in}\rangle$ or $|\Psi_{in}\rangle$ is prepared using fiber polarization controllers and wave plates. The bias phase α_0 of Eqs. 1 and 2 is directly controlled with one of the half–wave plates (HWPs) that are used to prepare the polarization of the pump beam, whereas the wavelengths of the photons are tuned with the temperature of the nonlinear down-conversion crystal to yield a range between 800 and 819 nm. More details on the spectral properties are provided in section B of the Supplementary Materials. To demonstrate the technique, we used sucrose solutions. Although sucrose solutions are not delicate, the choice of wavelength would be important for potential applications in biology because the damage to biological samples and losses are wavelength-dependent. In these matters, near-infrared light tends to strike a favorable balance between competing unwanted effects (*21*). The light-matter interaction takes place as both photons travel through the same sample, which provides a path length of 20 mm. The content of the cuvette is either water or a sucrose solution with a concentration of 0.200 ± 0.002 g/ml

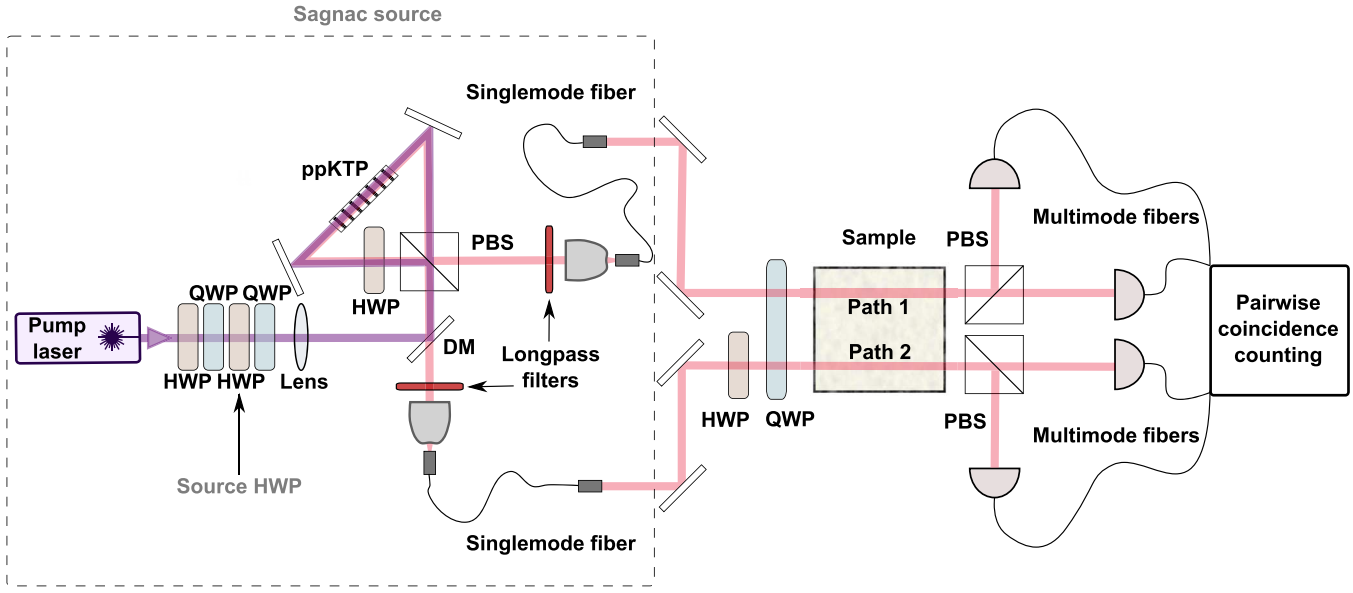

Fig. 2. Schematic of the experimental setup. Wavelength-tunable polarization-entangled photon pairs in separate paths are created by type II SPDC in a polarization-based Sagnac interferometer. The bias phase is controlled with the HWP labeled "Source HWP," which is in a set of four wave plates used to control the pump polarization (the first HWP controls the relative amplitude, and the Source HWP controls the relative phase between H and V). The preparation of the desired polarization state of the photon pair is then completed by a HWP and a quarter–wave plate (QWP) before the sample (the HWP setting determines whether $|\Phi_{in}\rangle$ in Eq. 1 or $|\Psi_{in}\rangle$ in Eq. 2 is selected). Next, the photons propagate through the sample, which consists of a cuvette with a path length of 20 mm filled with either water or a sucrose solution. Afterward, each photon is incident on a polarizing beam splitter (PBS), followed by multimode fiber coupling and detection with avalanche photodiodes (APDs). A coincidence logic enables the detection of the four types of coincidences in the H-V basis (HH, HV, VH, and VV). DM, dichroic mirror; ppKTP, periodically poled potassium titanyl phosphate.

or 0.400 ± 0.008 g/ml. After the cuvette, a projective measurement of the photon pair in the H-V basis is performed, using two PBSs and four APDs. Further technical details about the experimental setup can be found in Materials and Methods.

Calibration measurements

In preparation for the measurements of optical activity and optical rotatory dispersion of sucrose, a calibration was performed to determine the mapping from photon coincidence counts to phases and to assess the experimental sensitivity. Instead of using an optically active sample, the calibration was based on polarization control through HWPs in the setup, because this enabled a straightforward and wide tunability of the phases. The mapping was obtained through recording the coincidence counts as a function of the bias phase α_0. The experimental visibilities for the different wavelength settings of the experiment range from 91.4 to 93.6%.

The fitted sinusoidal calibration curves of the four types of coincidences from a measurement using $|\Psi_{in}\rangle$ at the degenerate wavelength (see section C of the Supplementary Materials) were used to infer the experimental FI. Figure 3 shows a comparison of the FI as a function of the rotation difference for three cases: the case of an ideal implementation of the proposed scheme with the entangled state $|\Psi_{in}\rangle$, the case of an ideal implementation of the classical scheme, and the inferred FI for the experimental implementation. The inferred experimental FI accounts for all the experimental details that lead to a reduced visibility but not for the losses, because it is based on data postselected for coincidences. Because the visibilities are below 100%, the experimental FI has a dependence on the value of the rotation difference and does not reach the ideal value for entangled photons. Nonetheless, for any given rotation difference, the bias phase can be used to shift the curve horizontally such that the experimental FI surpasses the classical FI. As the subsequent optical activity measurements involved small polarization rotations, the bias phase was adjusted to maximize the sensitivity for these main measurements.

Optical rotatory dispersion measurements

For the optical activity study, we measured the mean and difference of the optical rotations at five pairs of wavelengths, which are at varying distances from the degenerate wavelength 809.7 nm, and conducted these measurements using two different sucrose concentrations. A sequence of 7-min sets was taken, which consist of 1-s acquisitions recording the four types of coincidences. For each of the two input states, each of the two sucrose concentrations, and each of the five crystal temperatures used, one data set was taken with water and one was taken with a sucrose solution. The measurement results for mean rotations and rotation differences are shown in Fig. 4 (A and B, respectively). Overlaid are the curves predicted by an empirical model (section D of the Supplementary Materials). Because the optical activity is proportional to the concentration, for both means and differences, the values for the higher concentration of 0.4 g/ml are expected to be a factor of 2 larger than those for the lower concentration of 0.2 g/ml. The reason behind the mean rotations being approximately constant and the rotation differences being linear functions is that the optical rotatory dispersion curve is nearly linear within the spectral region that is probed (section D of the Supplementary Materials).

The graphs show the expected overall behavior, and the model notably has no free-fitting parameters. The systematic deviation in Fig. 4B for the concentration of 0.4 g/ml might be due to an unintended difference between conditions, for example, concentrations or other parameters that affect the rotations, for the two paths in the cuvette.

Apart from demonstrating the possibility of directly accessing the mean and difference rotation, it is also interesting to compare the experimental uncertainties with what could have ideally been achieved in the classical measurement. We calculated the classically achievable uncertainties using the Cramér-Rao bound (section A of the Supplementary Materials) for the given number of coincidences that were detected in the measurement sets belonging to the data points and compared them to the corresponding experimental values of the SEM. For the 20 data points in Fig. 4, the experimental SEM divided by the optimal uncertainty for the classical measurement is 0.77 ± 0.02.

DISCUSSION

This experiment is the first to use entangled photon states for quantum-enhanced differential measurements between different

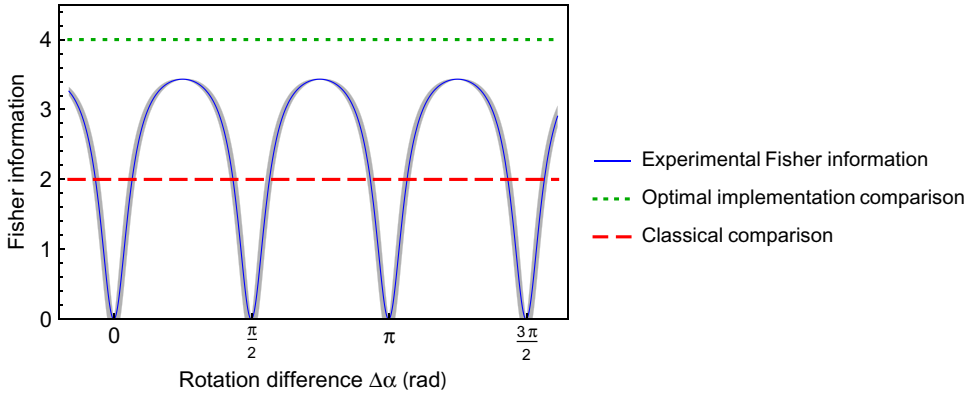

Fig. 3. Comparison of the FI as a function of the rotation difference for different lossless cases. The experimental FI inferred from the fitted sinusoidal curves of the calibration measurements for $|\Psi_{in}\rangle$, obtained with a HWP controlling the bias phase and converted to the equivalent values of $\Delta\alpha$, is shown as the solid blue line (section C of the Supplementary Materials). The narrow lighter blue–shaded region represents the uncertainty (± 1 SD), as obtained from the uncertainty of the fit parameters with standard uncertainty propagation. The inferred experimental FI is presented alongside the FI from an ideal implementation of the quantum measurement scheme (green dotted line) and the FI corresponding to an ideal classical measurement with linearly polarized photons (red dashed line).

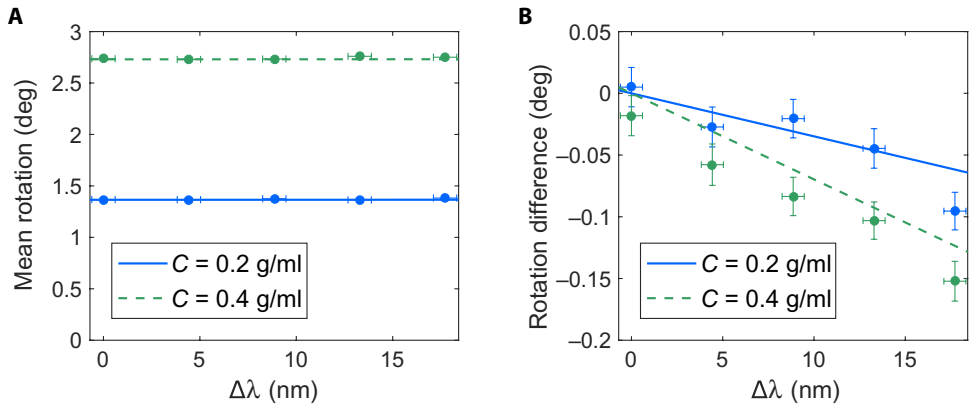

Fig. 4. Comparison of experimental optical activity measurement results (data points) for sucrose with predictions (lines). (**A** and **B**) The mean rotations obtained from using $|\Phi_{in}\rangle$ (A) and the rotation differences obtained from using $|\Psi_{in}\rangle$ (B), for wavelengths of 809.7 nm ± $\frac{\Delta\lambda}{2}$. The results for a concentration C = 0.4 g/ml are given by the dashed green line and those for C = 0.2 g/ml are given by the solid blue line. The horizontal error bars indicate ± 1 SD of the wavelength difference between the photons in a pair, estimated on the basis of the spectrum shown in fig. S1B. The vertical error bars show ± 1 SEM, estimated from the SD of the experimentally obtained angles. For the cases where the error bars are not clearly visible, the intervals are smaller than the markers. The measurements were taken at a temperature of 19°C and with a setting of the bias phase to maximize the FI.

wavelengths. Our application of the method to the phenomenon of molecular optical activity, where wavelength dependence is important, enabled us to measure the key quantity of optical rotatory dispersion.

Another interesting feature of the experiment is the use of distinguishable photons, because it is in contrast to most of the optical quantum metrology experiments. One of the exceptions was the 2013 experiment by Bell *et al.* (*22*), which also used multiwavelength entangled photons. In their experiment, the probe state was produced by four-wave mixing, and it was used to measure an optical path length in an interferometer, which is comparable to the part of our optical activity experiment where $|\Phi_{in}\rangle$ is used to measure the mean rotation. By exploiting the distinguishability of the photons, both experiments avoid the limitation in recording some of the measurement outcomes that occurs in schemes where indistinguishable photon pairs are split only probabilistically before measurement by non–photon-number–resolving detectors.

In our study of optical activity, measuring the difference between two wavelengths was of particular interest. However, the same method can also be used for more general differential measurements. As further examples involving optical activity, the current setup can be adapted to compare the concentrations or enantiomeric purities of two solutions by choosing the photons to be at the same wavelength and simply performing the differential measurement across two different solutions. In magnetometry, the possibility of probing spatial field gradients with macroscopic singlet states has been established (*18*, *23*). An extension to states involving more photons is also possible for optical measurements. Photonic singlet states of higher photon numbers produced in parametric down-conversion have been proposed for the measurement of symmetry-breaking effects (*24*). Whereas singlet states are invariant to rotations about any axis, another option for an extension to higher photon numbers is the family of states constructed as a superposition of the eigenstates corresponding to the minimum and maximum eigenvalues of the generator of the unitary transformation (*17*, *25*, *26*). Similar states have also been considered in the context of quantum clock synchronization (*27*, *28*).

MATERIALS AND METHODS

For the SPDC process, a narrowband continuous-wave laser (Ondax SureLock diode laser) with a wavelength of 404.85 nm and a power of 2.5 mW was used as the pump. The nonlinear crystal was a 15-mm-long ppKTP crystal, phase-matched for near-degenerate down-conversion at the pump wavelength.

When transitioning between different wavelength settings, the setup was left unchanged, except for the required shift in the crystal temperature, which was controlled with an oven, and an adjustment of the HWP that controlled the bias phase. This adjustment was found to be necessary to maintain a constant bias phase, most likely due to dispersive birefringent elements, such as wave plates, in the setup. Typical background-corrected visibilities of the biphoton state at the output from the Sagnac interferometer in the diagonal-antidiagonal basis were 97.99 ± 0.08%.

After coupling into singlemode fibers, unwanted polarization transformations in the fibers and subsequent mirrors were compensated for with fiber polarization controllers. As the last step before incidence on the sample, the state $\frac{1}{\sqrt{2}}[|H,\lambda_1\rangle_1|V,\lambda_2\rangle_2 - e^{i\alpha_0}|V,\lambda_1\rangle_1|H,\lambda_2\rangle_2]$ from the quantum source was transformed to the desired input states $|\Phi_{in}\rangle$ and $|\Psi_{in}\rangle$ using one of two settings of a HWP for one of the paths and a QWP for both paths.

For the sample, we used high-performance liquid chromatography–grade water (Hartenstein GmbH), and for the sucrose solutions, D(+)-Sucrose pure Ph. Eur., NF (Hartenstein GmbH) was dissolved in this water. Although the two photonic paths are drawn horizontally beside each other in Fig. 2 for clarity, the approximately 1-cm separation in our implementation was in fact vertical owing to the dimensions of the cuvette.

A number of measures were taken to stabilize the photon counts and polarizations within the experiment. In particular, the section of the setup containing the biphoton source was enclosed and insulated to minimize vibrations and temperature fluctuations. The temperature of the singlemode fibers was also stabilized with insulating tape.

Because standard equipment was used, there were considerable losses in the experiment: Without accounting for the singlemode

fiber coupling of the photons in the Sagnac source and for the detection efficiency of the APDs, the single-photon transmission through the setup was typically 46 to 56%. However, overall losses in the experiment could be significantly reduced by using high-efficiency detectors and antireflection-coated elements throughout. An improved efficiency would be required to enable quantum-enhanced precision when accounting for all of the photons used and not just the detected photons.

For the optical activity measurements that make up the results shown in Fig. 4, the average number of coincidences recorded per second was 1.837×10^4 and the total number of coincidences that contribute to each 7-min data set ($n = 40$ data sets) ranged between 7.287×10^6 and 8.203×10^6. An analysis of the noise, which showed that the coincidence counts were close to Poisson-distributed, is provided in section E of the Supplementary Materials.

Because accidental coincidences did not contribute to the sinusoidal signal with respect to the measured phase, they were one of the reasons for the nonunity fringe visibility, although imperfections in the state preparation were the primary reason. Accidentals were not subtracted as part of the analysis of the optical activity measurement data, because their effect was taken into account by the calibration curves (section C of the Supplementary Materials).

SUPPLEMENTARY MATERIALS

Supplementary material for this article is available at http://advances.sciencemag.org/cgi/content/full/2/10/e1601306/DC1

A. FI calculations
B. Spectral characterization of the biphoton state
C. Calibration curves
D. Optical activity predictions
E. Measurement noise
table S1. FI for three two-photon input states (columns) with respect to the two parameters of interest, namely, the mean rotation $\bar{\alpha}$ and rotation difference $\Delta\alpha$.
fig. S1. Spectral characterization of the photon pairs.
fig. S2. Calibration of the measurement outcome as a function of the phase in the biphoton state, which is controlled with the Sagnac source HWP.
fig. S3. Test of the experimental quantum state by rotating a HWP behind the sample at the degenerate wavelength setting.
fig. S4. Response of the classical state, consisting of a pair of linearly polarized photons at the degenerate wavelength setting, to the rotation of a HWP behind the sample.
fig. S5. Model of the optical activity of sucrose as a function of wavelength.
fig. S6. Experimental photon statistics.
References (*29*, *30*)

REFERENCES AND NOTES

1. W. J. Lough, I. W. Wainer, Eds., *Chirality in the Natural and Applied Science* (Blackwell Publishing Ltd., 2002).
2. D. B. Amabilino, *Chirality at the Nanoscale: Nanoparticles, Surfaces, Materials and More* (Wiley-VCH, 2009).
3. D. J. Caldwell, H. Eyring, *The Theory of Optical Activity* (Wiley-Interscience, 1971).
4. E. Charney, *The Molecular Basis of Optical Activity: Optical Rotatory Dispersion and Circular Dichroism* (Wiley, 1979).
5. L. D. Barron, *Molecular Light Scattering and Optical Activity* (Cambridge Univ. Press, 2004).
6. A. Kuzmich, L. Mandel, Sub-shot-noise interferometric measurements with two-photon states. *Quantum Semiclassical Opt.* **10**, 493–500 (1998).
7. M. W. Mitchell, J. S. Lundeen, A. M. Steinberg, Super-resolving phase measurements with a multiphoton entangled state. *Nature* **429**, 161–164 (2004).
8. F. W. Sun, B. H. Liu, Y. X. Gong, Y. F. Huang, Z. Y. Ou, G. C. Guo, Experimental demonstration of phase measurement precision beating standard quantum limit by projection measurement. *Europhys. Lett.* **82**, 24001 (2008).
9. B. L. Higgins, D. W. Berry, S. D. Bartlett, M. W. Mitchell, H. M. Wiseman, G. J. Pryde, Demonstrating Heisenberg-limited unambiguous phase estimation without adaptive measurements. *New J. Phys.* **11**, 073023 (2009).
10. G. Y. Xiang, B. L. Higgins, D. W. Berry, H. M. Wiseman, G. J. Pryde, Entanglement-enhanced measurement of a completely unknown optical phase. *Nat. Photonics* **5**, 43–47 (2011).
11. I. Afek, O. Ambar, Y. Silberberg, High-NOON states by mixing quantum and classical light. *Science* **328**, 879–881 (2010).
12. F. Wolfgramm, C. Vitelli, F. A. Beduini, N. Godbout, M. W. Mitchell, Entanglement-enhanced probing of a delicate material system. *Nat. Photonics* **7**, 28–32 (2013).
13. G. Y. Xiang, H. F. Hofmann, G. J. Pryde, Optimal multi-photon phase sensing with a single interference fringe. *Sci. Rep.* **3**, 2684 (2013).
14. Y. Israel, S. Rosen, Y. Silberberg, Supersensitive polarization microscopy using NOON states of light. *Phys. Rev. Lett.* **112**, 103604 (2014).
15. T. Ono, R. Okamoto, S. Takeuchi, An entanglement-enhanced microscope. *Nat. Commun.* **4**, 2426 (2013).
16. P. Kok, B. W. Lovett, *Optical Quantum Information Processing* (Cambridge Univ. Press, 2010).
17. V. Giovannetti, S. Lloyd, L. Maccone, Advances in quantum metrology. *Nat. Photonics* **5**, 222–229 (2011).
18. G. Tóth, I. Apellaniz, Quantum metrology from a quantum information science perspective. *J. Phys. A: Math. Theor.* **47**, 424006 (2014).
19. T. Kim, M. Fiorentino, F. N. C. Wong, Phase-stable source of polarization-entangled photons using a polarization Sagnac interferometer. *Phys. Rev. A* **73**, 012316 (2006).
20. A. Fedrizzi, T. Herbst, A. Poppe, T. Jennewein, A. Zeilinger, A wavelength-tunable fiber-coupled source of narrowband entangled photons. *Opt. Express* **15**, 15377–15386 (2007).
21. M. A. Taylor, W. P. Bowen, Quantum metrology and its application in biology. *Phys. Rep.* **615**, 1–59 (2016).
22. B. Bell, S. Kannan, A. McMillan, A. S. Clark, W. J. Wadsworth, J. G. Rarity, Multicolor quantum metrology with entangled photons. *Phys. Rev. Lett.* **111**, 093603 (2013).
23. I. Urizar-Lanz, P. Hyllus, I. L. Egusquiza, M. W. Mitchell, G. Tóth, Macroscopic singlet states for gradient magnetometry. *Phys. Rev. A* **88**, 013626 (2013).
24. H. Cable, G. A. Durkin, Parameter estimation with entangled photons produced by parametric down-conversion. *Phys. Rev. Lett.* **105**, 013603 (2010).
25. V. Giovannetti, S. Lloyd, L. Maccone, Quantum metrology. *Phys. Rev. Lett.* **96**, 010401 (2006).
26. M. Zwierz, C. A. Pérez-Delgado, P. Kok, Ultimate limits to quantum metrology and the meaning of the Heisenberg limit. *Phys. Rev. A* **85**, 042112 (2012).
27. R. Jozsa, D. S. Abrams, J. P. Dowling, C. P. Williams, Quantum clock synchronization based on shared prior entanglement. *Phys. Rev. Lett.* **85**, 2010 (2000).
28. Y.-L. Zhang, Y.-R. Zhang, L.-Z. Mu, H. Fan, Criterion for remote clock synchronization with Heisenberg-scaling accuracy. *Phys. Rev. A* **88**, 052314 (2013).
29. A. Crespi, M. Lobino, J. C. F. Matthews, A. Politi, C. R. Neal, R. Ramponi, R. Osellame, J. L. O'Brien, Measuring protein concentration with entangled photons. *Appl. Phys. Lett.* **100**, 233704 (2012).
30. T. M. Lowry, E. M. Richards, CCCXLVI.—The rotatory dispersive power of organic compounds. Part XIII. The significance of simple rotatory dispersion. Rotatory dispersion of camphorquinone and of sucrose. *J. Chem. Soc. Trans.* **125**, 2511–2524 (1924).

Acknowledgments: We thank A. Bismarck and the Polymer and Composite Engineering group of the University of Vienna for access to laboratory equipment. N.T. further thanks W. Plick, D. Berry, and A. Gilchrist for helpful discussions. **Funding:** The project was supported by the Austrian Academy of Sciences (ÖAW), the Austrian Science Fund (FWF) with SFB F40 (FOQUS), the Australian Research Council's Centre of Excellence for Engineered Quantum Systems (EQuS) grant no. CE110001013, and the Australian Research Council's Discovery Project (DP160103332). G.M.-T. was also supported through an Australian Research Council Future Fellowship. **Author contributions:** N.T. devised the scheme and designed the experiment, supported by the other authors. N.T. and R.F. built the experimental setup. N.T. performed the experiment and analyzed the data, with input from M.K., X.V., G.M.-T., and A.Z. N.T. wrote the manuscript, with input from the rest of the authors. A.Z. and G.M.-T. oversaw the work. **Competing interests:** The authors declare that they have no competing interests. **Data and materials availability:** All data needed to evaluate the conclusions in the paper are present in the paper and/or the Supplementary Materials. Additional data related to this paper may be requested from the authors.

Submitted 9 June 2016
Accepted 30 August 2016
Published 5 October 2016
10.1126/sciadv.1601306

Citation: N. Tischler, M. Krenn, R. Fickler, X. Vidal, A. Zeilinger, G. Molina-Terriza, Quantum optical rotatory dispersion. *Sci. Adv.* **2**, e1601306 (2016).